Available online at www.sciencedirect.com
ScienceDirect
Journal of the European Ceramic Society 31 (2011) 2357–2364
www.elsevier.com/locate/jeurceramsoc

Original article

New NO_x sensors based on hematite doped with alkaline and alkaline-earth elements

J.-M. Tulliani [a,*], C. Baroni [a], C. Lopez [b], L. Dessemond [b]

[a] *Materials Science and Chemical Engineering Department, Politecnico di Torino, Corso Duca degli Abruzzi 24, 10129 Torino, Italy*
[b] *LEPMI, UMR 5279, CNRS – Grenoble INP – Université de Savoie – Université Joseph Fourier, BP75, 38402 Saint Martin d'Hères, France*

Received 28 March 2011; received in revised form 10 May 2011; accepted 20 May 2011
Available online 17 June 2011

Abstract

Alkaline (lithium, potassium, rubidium) and alkaline-earth (magnesium, barium) doped hematite materials were studied for NO_2 sensing application. The synthesized materials were characterized by laser granulometry, X-ray diffraction and scanning electronic microscopy. A temperature of 1300 °C was chosen as the optimal heat treatment in order to obtain the densest material. Humidity dependence of the electrical properties revealed a strong influence in the case of rubidium doped hematite material while the other doped materials were less sensitive.

The AC impedance analyses underlined the n-type intrinsic semi-conduction of pure hematite. Alkaline-earth doped hematite materials showed two semi-conducting regions, below and above 500 °C, corresponding to extrinsic and intrinsic n-type semi-conduction, respectively. These electrical analyses associated with SEM observations suggested instability of the ferrites formed in rubidium and potassium doped materials.

AC electrical measurements were performed in the 0–500 ppm NO_2 partial pressure range. The alkaline-earth doped hematite materials exhibited the most promising behavior.

Keywords: B. Structure and microstructure: spectroscopy; C. Properties: electrical conductivity; D. Compositions: ferrites; E. Applications: sensors; NO_2 detection

1. Introduction

The term NO_x indicates a mixture of NO and NO_2 that is generated by hydrocarbons combustion at high temperatures. Nitrogen oxides are mainly emitted from automobiles, stationary combustion facilities and home equipments. These emissions contribute to form acid rains and the photochemical smog that may cause harm to breathing apparatus and eyes.

The current directive 2008/50/EC of the European Union on ambient air quality has set at 40 $\mu g/m^3$ the annual limit value, and at 200 $\mu g/m^3$ the hourly limit value, not to be exceeded more than 18 times in a calendar year, for the protection of human health against the effects of gaseous NO_2.[1]

Measurements of NO_x concentrations have been done so far by means of spectroscopic instruments based on chemical luminescence[1] or infrared absorption, however such instruments do not allow on-site monitoring. There is then a growing interest in NO_x sensors able to operate within combustion exhaust gases. Crucial parameters for this type of sensors are: sensitivity, accuracy and stability, as well as low cost.[2]

In this work, alkaline and alkaline-earth doped hematite were investigated as potential NO_x sensing materials able to work in the exhaust gases of gas boilers. The properties of doped α-Fe_2O_3 and of ferrites have been studied in detail especially as humidity sensors based on: iron oxide,[3,4] $MgFe_2O_4$,[5] $MgFe_2O_4$–CeO_2,[6] Li–doped Fe_2O_3,[7,8] K, Na, Mg, Ca, Rb, Ba, Sr-doped Fe_2O_3,[8] Zn^{2+} and Au^{3+}-doped Fe_2O_3,[9] Au-doped $LiFe_2O_3$,[10] Li substituted Mg-ferrite,[11] Fe_2O_3 nanoparticles on sepiolite,[12] K^+-β-ferrite,[13] and silica–Fe_2O_3.[14]

Several Fe_2O_3 compounds have been also investigated as NO_x sensors such as: sol–gel derived α-Fe_2O_3 thin film,[15] Nb-doped α-Fe_2O_3,[16] $ZnFe_2O_4$,[17] Au and Zn-doped Fe_2O_3,[18] Zn-doped γ-Fe_2O_3,[19] and Fe_2O_3-In_2O_3.[20]

Hematite and doped hematite are excellent humidity sensor, whereas alkaline or alkaline-earth-doped hematite (α-Fe_2O_3) materials have not been investigated yet in the literature, as NO_x sensors. So, the aims of this work were to prepare alkaline and alkaline-earth-doped hematite NO_x sensors and to investigate the

* Corresponding author. Tel.: +39 (0)11 564 47 00; fax: +39 (0)11 564 46 99.
E-mail address: jeanmarc.tulliani@polito.it (J.-M. Tulliani).

0955-2219/$ – see front matter © 2011 Elsevier Ltd. All rights reserved.
doi:10.1016/j.jeurceramsoc.2011.05.031

electrical properties of these materials by means of impedance spectroscopy.

2. Experimental

α-Fe_2O_3 powder (Aldrich >99%, particle size distribution below 2 μm) was mixed in ethanol with carbonates used as precursors of 5 wt% equivalent of lithium, potassium, rubidium, magnesium and barium oxides (all Fluka >99%), in a planetary mill, in agate jars with agate balls, for 3 h. After drying overnight in an oven, the mixtures were uniaxially pressed at 370 MPa and calcined at 900 °C for 1 h. Then, the samples were first manually ground with an agate mortar and an agate pestle, prior to planetary mill them for 6 h in agate jars with agate balls. The grain size of the produced powders was then controlled by laser granulometry (Fritsch analysette 22). The retained solution was to increase the green density of the pellets by adding polyethylene glycol (PEG 4000, Sigma–Aldrich) to the doped powder, during the 6 h planetary milling step. Pellets were uniaxially pressed at 370 MPa and heat treated between 1000 and 1300 °C for 1 h, with an heating ramp of 5 °C/min. This sintering temperature was chosen because relative densities as high as 98% of theoretical one (5.27 g/cm^3) were obtained with pure hematite.

The fired materials were characterized by XRD (Philips PW1710) in the 5–70° range, after calcination at 900 °C and sintering at 1300 °C.

The sintering temperature was chosen after a study of the density evolutions for all the samples. Before the electrical characterization, the materials were observed by means of a scanning electron microscope (SEM, Hitachi S2300).

The samples were first studied as humidity sensors in preliminary tests, because it is known in the literature that water molecules can interfere with NO_x detection.

Interdigitated gold electrodes (ESL 520 A) were screen-printed onto the surface of the pellets and the sensors humidity response was studied in the range 0–100% relative humidity (RH) in a laboratory apparatus. In this chamber, compressed air was separated into two fluxes: one was dehydrated over a chromatography alumina bed while the second one was directed through two water bubblers, generating, respectively, a dry and a humid flow. Two precision microvalves allowed to recombine the two fluxes into one by means of a mixer and to adjust the RH content while keeping constant the testing conditions: a flow rate of 0.05 L/s. The relative humidity was not increased in a continuous mode but was varied by steps. The measurements were performed at room temperature. A commercial humidity and temperature probe was used as a reference for temperature and RH values (Delta Ohm HD2101.1), accuracy: ±0.1% in the 0–100% RH range and −50 to 250 °C temperature range. Each tested sensor was alimented by an external alternating voltage (V = 3.6 V at the rate of 1 kHz) and then constituted a variable resistance of this electrical circuit. A multimeter (Keithley 2000) was used to measure the tension V_{DC} at the output of the circuit. The sensor resistance was determined by substituting them, in the circuit, by known resistances and then plotting a calibrating curve $R = f(V_{DC})$.

Table 1
Phases detected in doped hematite samples.

Sample	Phases	JCPDS card
Fe_2O_3	α-Fe_2O_3	33-0664
Fe_2O_3 + 5 wt% Li_2O	$LiFe_5O_8$	38-0259
Fe_2O_3 + 5 wt% K_2O	α-Fe_2O_3	33-0664
	$KFe_{11}O_{17}$	25-0651
Fe_2O_3 + 5 wt% Rb_2O	α-Fe_2O_3	33-0664
	Rb-$\beta''$$Fe_2O_3$	/
Fe_2O_3 + 5 wt% MgO	α-Fe_2O_3	33-0664
	$MgFe_2O_4$	36-0398
Fe_2O_3 + 5 wt% BaO	α-Fe_2O_3	33-0664
	$BaFe_{12}O_{19}$	39-1433

Subsequently, the electrical characterization of the materials was performed by means of AC impedance spectroscopy after painting platinum electrodes (ESL 5545) onto each face of the pellets (∼1 cm in diameter and ∼1 mm thick). These measurements were carried out under dry synthetic air (80% N_2–20% O_2; Messer) and argon (<2×10^{-6} atm O_2; Air Liquide), between 100 and 700 °C, in the 5 Hz to 13 MHz frequency range and a 100 mV amplitude signal (Hewlett Packard HP 4192A LF Impedance Analyzer).

A strong dependence of the resistance due to the presence of residual hydroxyl groups onto the surface of the pellets was evidenced. A previously heating treatment up to 700 °C was then applied before each electrical analysis. This latter consisted in a succession of AC impedance measurements during cooling and heating, under the same gas atmosphere in order to verify the reproducibility of each result.

The NO_2 responses of the materials were determined by the total resistance measured in mixed flux of helium (Messer) and N_2/1000 ppm NO_2 (Air Liquide). Finally, the electrical measurements were performed in the 0–500 ppm NO_2 partial pressure range with the impedance meter and the parameters described above.

The sensor response SR was calculated on the basis of equation (1):

$$\mathrm{SR} = \frac{R_{(P_{\mathrm{gas}})} - R_{(P_{\mathrm{gas}} \to 0)}}{R_{(P_{\mathrm{gas}} \to 0)}} \quad (1)$$

where $R_{(P_{\mathrm{gas}})}$ is the total resistance of the material when exposed under $P_{(\mathrm{gas})}$ partial pressure and $R_{(P_{\mathrm{gas}} \to 0)}$ is the measured resistance deduced from the $R_{(P_{NO_2})}$ representation (not presented in this paper) when the gas partial pressure tends towards zero.

3. Results

After the first thermal treatment at 900 °C and the 6 h planetary milling, the powders showed a mean diameter of 2.15 μm for K, Mg, Rb doped hematite samples, 3.40 μm for Ba doped hematite and 7.05 μm for Li doped hematite samples. These values are comparable to the mean diameter of the starting α-Fe_2O_3 powder (2 μm).

X-ray diffraction patterns (Fig. 1, Table 1) on the crushed pellets of the doped hematite, after the first thermal treatment at 900 °C for 1 h, evidenced that the following ferrites were formed,

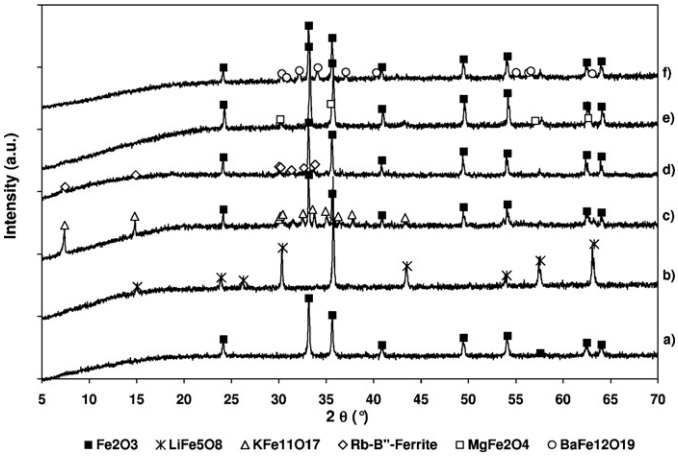

Fig. 1. XRD patterns of the samples fired at 900 °C: a) pure α-Fe_2O_3; b) α-Fe_2O_3 + 5% Li_2O; c) α-Fe_2O_3 + 5% K_2O; d) α-Fe_2O_3 + 5% Rb_2O; e) α-Fe_2O_3 + 5% MgO and f) α-Fe_2O_3 + 5% BaO.

after lithium, barium, magnesium, potassium and rubidium additions, respectively: $LiFe_5O_8$, $BaFe_{12}O_{19}$, $MgFe_2O_4$, $KFe_{11}O_{17}$ and Rb-β″-ferrite. While with lithium doping, only lithium iron oxide was detected, as also expected from the determination of the theoretical ferrite content within each sample (Table 2).

Geometrical density evolution was studied in function of the sintering temperature in the 1000–1300 °C temperature range. As expected, the highest densities were obtained with the 1300 °C thermal treatment.

The theoretical densities of the samples fired at 1300 °C were expressed considering the different phases within all the samples, as evidenced by X-ray diffraction and assuming that all the ferrite that could be formed was effectively formed. These values are reported in Table 2.

The correlation between humidity sensor response and the material porosity is known in the literature, and it is possible to evaluate the pore radius at which capillary condensation occurs at different temperatures (T) by means of the Kelvin equation[21]:

$$r_k = \frac{2\gamma M}{\rho RT \ln(P/P_S)} \quad (2)$$

where r_k is the pore radius, γ, ρ, M are, respectively, the water surface tension, density and molecular weight, while P and P_S are the water vapor pressures in the surrounding atmosphere and at saturation, respectively. Because the porous structure of ceramics with open pores tends to favor water and gases adsorption and condensation, and though, on semiconducting materials these features are less critical,[4] the efforts were oriented on the reduction of the sensors porosity, as in general, dense ceramics show negligible humidity–sensitivity.[22]

Table 2
Density of doped samples sintered at 1300 °C.

Sample	Expected ferrite (wt%)	Geometrical density (g/cm^3)	Relative density (%)
Fe_2O_3	0	5.11 ± 0.05	98.3
Fe_2O_3 + 5 wt% Li_2O	98.6	4.53 ± 0.05	95.9
Fe_2O_3 + 5 wt% K_2O	43.9	3.97 ± 0.05	81.9
Fe_2O_3 + 5 wt% Rb_2O	30.6	4.83 ± 0.05	/
Fe_2O_3 + 5 wt% MgO	24.8	4.75 ± 0.05	93.6
Fe_2O_3 + 5 wt% BaO	36.2	5.08 ± 0.05	96.4

Table 3
Activation energies extract from the linear regions of Fig. 4.

	Activation energy (eV)			
	Below 500 °C		Above 500 °C	
	Argon	Air	Argon	Air
α-Fe_2O_3		0.71		
Fe_2O_3–5% Li_2O	0.62	0.73	0.22	0.41
Fe_2O_3–5% K_2O		0.45		
Fe_2O_3–5% Rb_2O		0.81		
Fe_2O_3–5% MgO	0.30	0.40	0.15	0.17
Fe_2O_3–5% BaO	0.38	0.53	0.26	0.28

It was then decided, from now on, to fire all the sensors at the highest temperature (1300 °C), in order to have the densest samples as possible.

Microstructures of the materials fired at 1300 °C were observed by means of a SEM (Fig. 2) and the rather high densities of the materials were confirmed, in particular for pure hematite and for barium, rubidium and magnesium-doped compositions.

In potassium, magnesium and barium doped hematite samples, two different microstructures were present: the hematite one, made of rather hexagonal grains and the ferrites $KFe_{11}O_{17}$, Rb-β″-ferrite, $MgFe_2O_4$ and $BaFe_{12}O_{19}$, characterized by lamellar grains. On the contrary, in lithium-doped samples the grains were quite regular.

In Fig. 2, as the grain sizes were significantly different between the various samples, it was not possible to use the same magnification for all SEM micrographs.

The sensor responses SR of the previously described materials as a function of the relative humidity are presented in Fig. 3. The pure, as well as, the magnesium doped hematite materials show a slight increase of their electrical resistances above ca. 80 RH% while the resistance of the rubidium doped hematite material strongly depends on the relative humidity even for low RH values. This strong dependence of its resistance with relative humidity eliminates the rubidium doped hematite regarding a selective sensitivity of this material for a NO_2 sensing application. The potassium and lithium-doped hematite were also rather sensitive to water vapor above ca. 55 and 80 RH%, respectively.

On the contrary, the SR dependence of the barium doped hematite material with relative humidity is too small to be measured.

Fig. 4 shows the conductivities evolutions in Arrhenius representations of pure hematite and the 5 alkaline and alkaline-earth doped hematite samples. The conductivities were calculated on the basis of the total resistance measured by means of AC impedance spectroscopy. The impedance measurements have been realized under synthetic air and argon atmospheres successively.

Table 3 summarizes the values of activation energies, deduced from the linear regions of the 6 Arrhenius representations presented in Fig. 4.

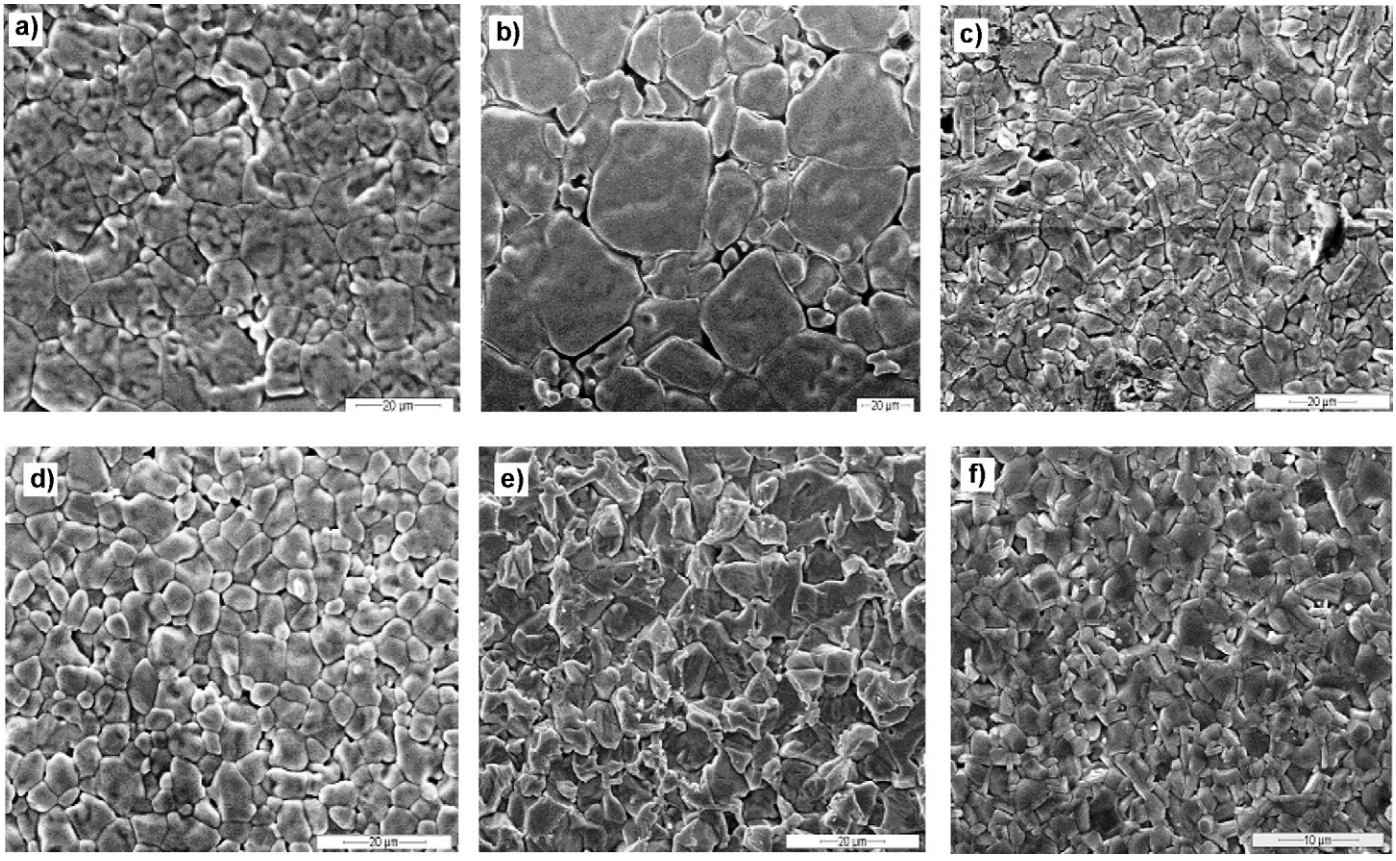

Fig. 2. SEM micrographs of sintered samples: a) α-Fe_2O_3 pure (1000×); b) α-Fe_2O_3 + 5% Li_2O (600×); c) α-Fe_2O_3 + 5% K_2O (800×); d) α-Fe_2O_3 + 5% Rb_2O (1000×); e) α-Fe_2O_3 + 5% MgO (800×) and f) α-Fe_2O_3 + 5% BaO (2000×).

The case of potassium and rubidium doped hematite materials is more difficult to analyze. These materials showed a rapid degradation of the formed ferrites with re-precipitation phenomena on the pellets surfaces (Fig. 5).

Except potassium doped hematite material which did not give a significant response, pure hematite, alkaline and alkaline earth doped hematite materials were tested under NO_2 partial pressure (0–500 ppm) in the 60–350 °C temperature range.

Fig. 6 represents the evolution of the sensor response for $P_{NO_2} = 400$ ppm. For temperatures above 350 °C most of the materials exhibited a poor NO_2 response. For temperatures below 200 °C the impedance of most of them were too high (and also the uncertainties) to permit a quantitative determination of the total resistance. Considering the highest sensitivity (slope of the representation $SR(P_{NO_2})$) and the lowest uncertainties, the optimal temperature is estimated to be 250 °C.[15,18,23,24]

Fig. 7 gathers the representations $SR(P_{NO_2})$ measured at 250 °C. We did not take into account the points measured in pure helium atmosphere ($P_{NO_2} = 0$ ppm) considering the uncertainty of their values. Furthermore the points measured for $P_{NO_2} = 500$ ppm frequently showed a saturation phenomenon. This latter is noteworthy for magnesium and barium doped hematite materials for which the representations are particularly linear. Table 4 summarizes the values of sensitivity (slope of the $SR(P_{NO_2})$ representation) and resistance $R(P_{NO_2 \to 0})$.

4. Discussion

Fig. 4 shows two types of electrical behaviors. Pure hematite as well as potassium and rubidium doped hematite samples present a linear dependence of the conductivity with superimposition of the measurements under air and argon. In the case of lithium, magnesium and barium doped hematite materials no influence of the oxygen partial pressure above 500 °C

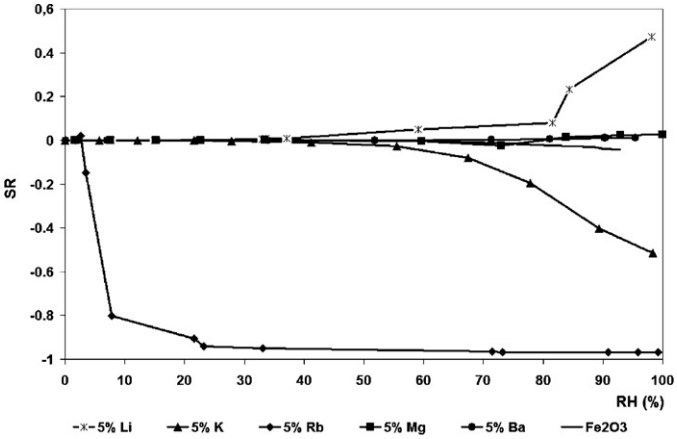

Fig. 3. Sensors response (SR) in function of RH, at 20 °C, for the samples fired at 1300 °C.

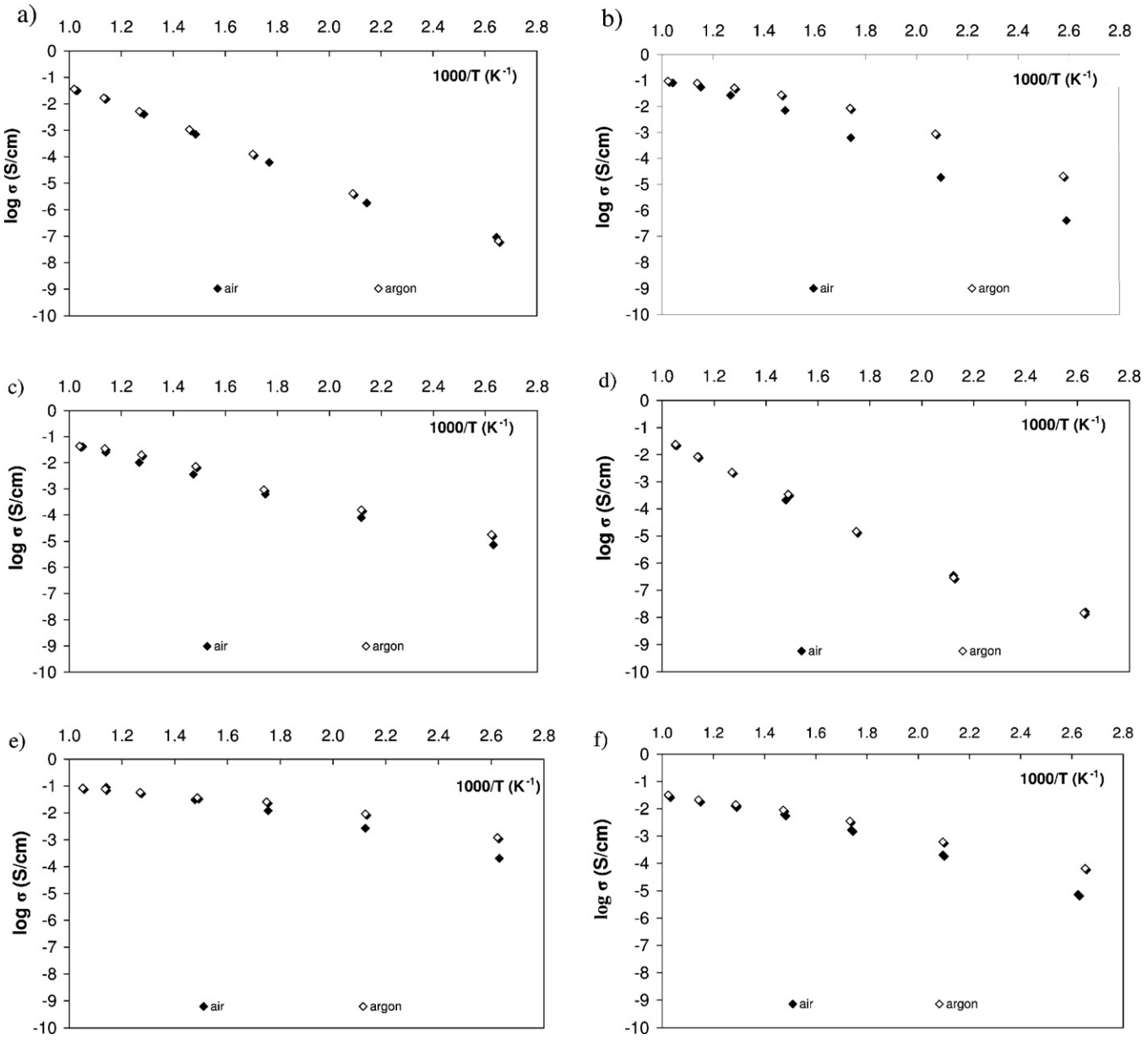

Fig. 4. Arrhenius diagram of the conductivity under dry air ♦and argon ◊: a) α-Fe_2O_3 pure; b) α-Fe_2O_3 + 5% Li_2O; c) α-Fe_2O_3 + 5% K_2O; d) α-Fe_2O_3 + 5% Rb_2O; e) α-Fe_2O_3 + 5% MgO; and f) α-Fe_2O_3 + 5% BaO.

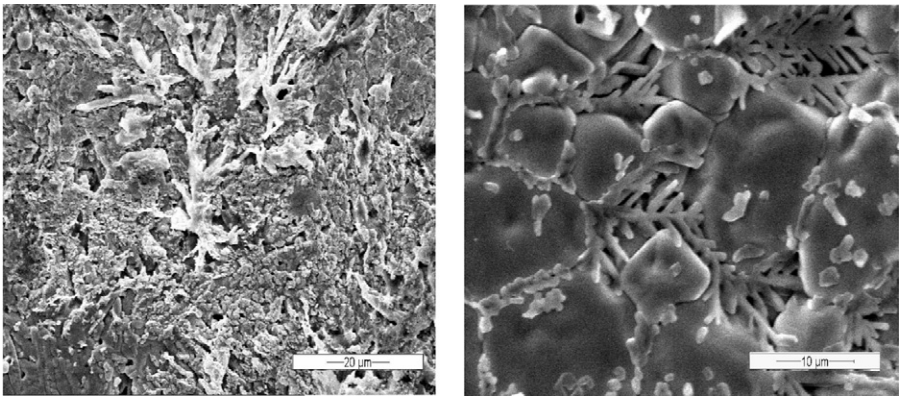

Fig. 5. SEM micrographs of degradation products on the sample surfaces: α-Fe_2O_3 + 5% K_2O (800×) on the left and α-Fe_2O_3 + 5% Rb_2O (2000×) on the right.

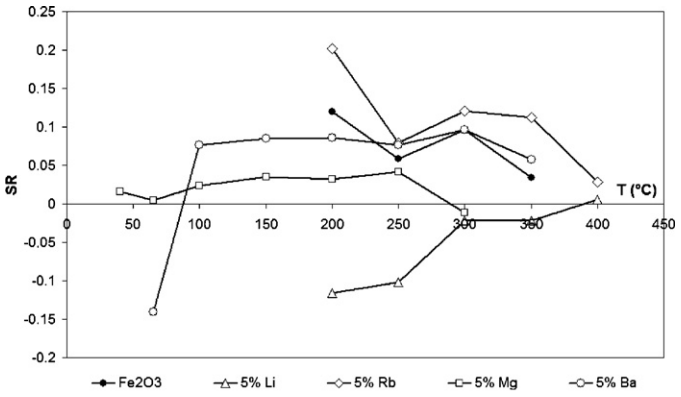

Fig. 6. Sensor response (SR) of alkaline and alkaline earth doped hematite materials in function of temperature for $P_{NO_2} = 400$ ppm.

(below $1000/T = 1.3\,K^{-1}$) is observed, while a strong influence of the oxygen partial pressure below 500 °C (above $1000/T = 1.3\,K^{-1}$) is evidenced. Furthermore, these three latter samples exhibit two linear regions (below and above 500 °C).

The n-type semiconducting behavior of hematite is clearly reported in literature.[25] Oxygen vacancies (V''_O) can be produced by heating this material following the disorder equation (3)[26]:

$$O_O^X = \frac{1}{2}O_{2(g)} + V''_O + 2\acute{e} \quad (3)$$

Gardner et al.[27] measured the oxygen deficit resulting from this equilibrium shift. Considering this structural disorder and the independence of the hematite conductivity regarding the oxygen partial pressure shown in Fig. 5a, we can conclude that this material is an intrinsic semiconductor.[26,28] The large value of

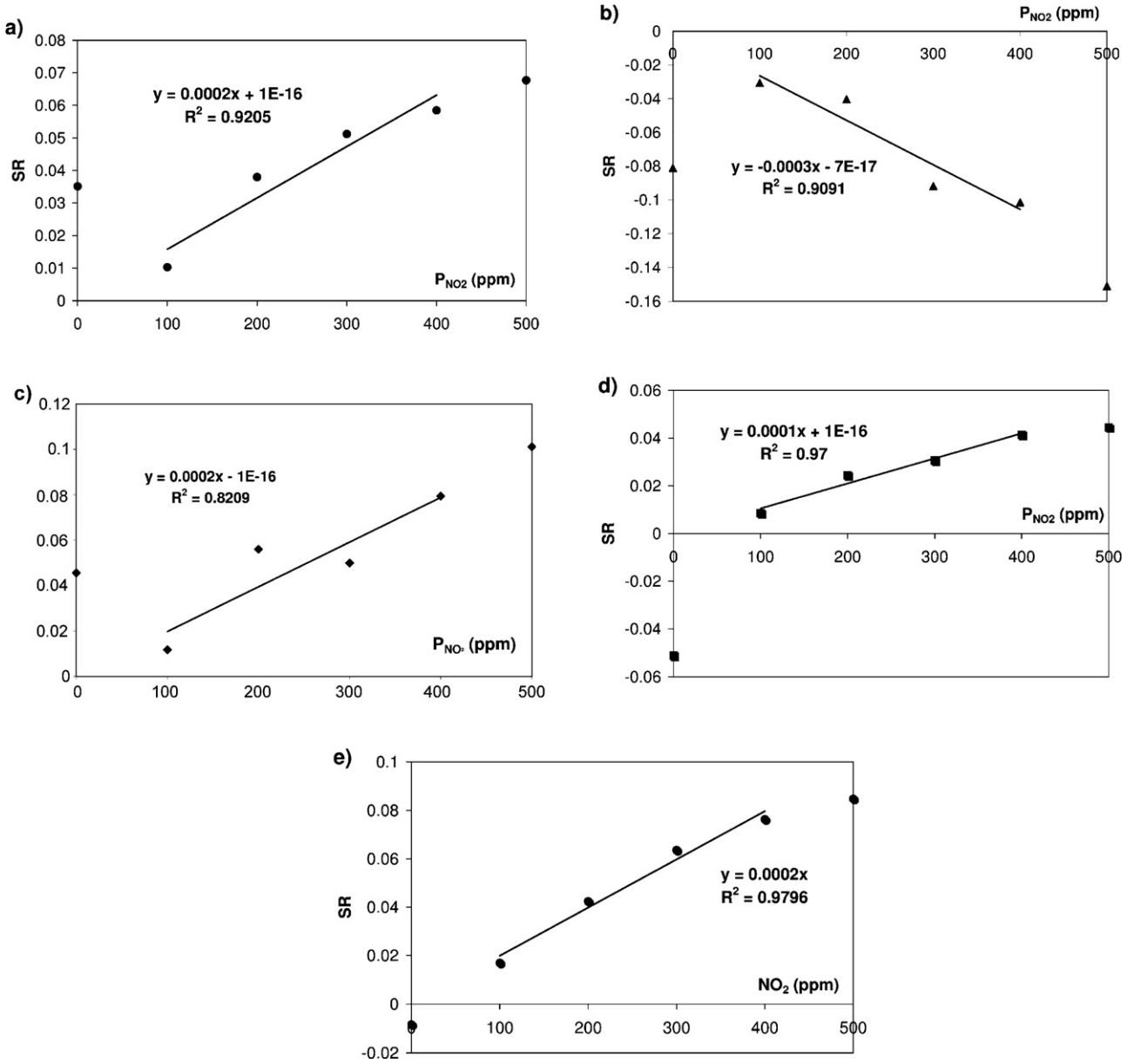

Fig. 7. Sensor response (SR) in function of NO_2 partial pressure at 250 °C: a) α-Fe_2O_3 pure; b) α-Fe_2O_3 + 5% Li_2O; c) α-Fe_2O_3 + 5% Rb_2O; d) α-Fe_2O_3 + 5% MgO; and e) α-Fe_2O_3 + 5% BaO.

Table 4
Sensitivity (S) of the different hematite and doped hematite of this work measured at 250 °C.

Sample	S (ppm^{-1})	$R(P_{NO_2 \to 0})$ (Ω)
Fe_2O_3	1.6×10^{-4}	8134
Fe_2O_3 + 5 wt. eq.% Li_2O	-2.6×10^{-4}	1029
Fe_2O_3 + 5 wt. eq.% Rb_2O	2×10^{-4}	11525
Fe_2O_3 + 5 wt. eq.% MgO	10^{-4}	6.84
Fe_2O_3 + 5 wt. eq.% BaO	2×10^{-4}	236

activation energy measured in this work (0.71 eV) is the consequence of our experimental procedure where samples were sintered at 1300 °C and cooled under air laboratory. Under those conditions, the oxygen vacancies created during the heat treatment disappear by re-oxidation[27] and hematite becomes a slight n-type semiconductor.[29] The value of 0.71 eV obtained in the present work is close from the one reported by Gardner et al.[27]

Conductivity of lithium, magnesium and barium doped hematite materials show a large dependence with oxygen partial pressure for temperatures below 500 °C. Furthermore, the conductivities increase as the oxygen partial pressure decreases. The conductivities under argon are higher than the conductivities under air. This corresponds to the behavior of a n-type extrinsic semiconductor. Kim et al.[26] suggested a doping process with reduction of a part of Fe(III) to Fe(II), oxygen vacancies formation and concentration increase of negative charge carriers (electrons). They also suggested that the semiconducting behavior became intrinsic for temperature above 500 °C. We observe the same phenomenon and the activation energies deduced from Fig. 4b, e and f are close from the values obtained by Gardner et al.[27] on pure hematite in the same temperature range (0.1–0.3 eV).

The case of potassium and rubidium doped hematite materials is more difficult to analyze, because of the rapid degradation of the formed ferrites, as above mentioned (Fig. 5). The observed crystals are probably alkaline carbonates.

The electrical consequence is particularly evident for rubidium doped hematite which behaves like pure hematite. The case of potassium doped hematite is somewhat different because its activation energy is lower than a pure hematite one's and it presents a slight n-type extrinsic semiconducting behavior (the conductivity under argon is higher than under air). Authors[30,31] suggested a mixed ionic and electronic conductivity for potassium ferrite. The total conductivity we obtain at 300 °C (10^{-3} S/cm) is close from Ito's value (3.53×10^{-3} S/cm). As for them, they attributed this value to ionic conductivity. But we have to take precautions with the electrical results obtained for rubidium and potassium doped hematite materials because of the degradation of the samples. Potassium and rubidium ferrites are affected by hydrolysis and produce γ-Fe_2O_3.[32]

A qualitative analysis of the SR evolution with temperature from Fig. 6 allows to observe that the behavior of pure hematite and rubidium doped hematite materials are similar. This confirms that rubidium doped hematite material behaves as pure hematite and that α-Fe_2O_3 + 5 wt% Rb_2O is not stable (hydrolysis phenomena suggested above). We can also notice the similar behavior of magnesium and barium doped hematite materials. Finally, lithium doped hematite material exhibits an original evolution that can be explained in terms of the transition from n-to p-type conductivity.[33] The changing of the behavior of some oxides is caused by the formation of an inversion layer on their surface due to oxygen adsorption.[33]

In Fig. 7, except for lithium doped hematite, all other materials present a resistance increase as the NO_2 partial pressure increases. This result has already been observed with hematite and various ferrites.[15,18,24,34]

In a n-type semiconductor, NO_2 does not react with preadsorbed oxygen and resistance changes occur by a direct chemisorption process.[35] A series of reactions giving nitrates and nitrites is proposed in ref.[36]:

$$NO_2 + e^- \text{ (c.b.)} \leftrightarrow NO_2^- \quad (4a)$$

$$NO_2 + V_O^+ \leftrightarrow NO_2^- + V_O^{2+} \quad (4b)$$

$$2NO_2 + O_2^- + e^- \text{ (c.b.)} \leftrightarrow 2NO_3^- \quad (5a)$$

$$2NO_2 + O_2^- + V_O^+ \text{ (c.b.)} \leftrightarrow 2NO_3^- + V_O^+ \quad (5b)$$

$$NO_2 + O^- \leftrightarrow NO_3^- \quad (6)$$

In surface reactions (4a), (4b), (5a) and (5b), electrons from the conduction band (c.b.) are trapped when surface species are formed, but not in reaction (6). If nitrates are formed by the last mechanism, a further equilibrium has to be considered, that is to say NO_3^- dissociation:

$$NO_3^- + e^- \text{ (c.b.)} \leftrightarrow NO + 2O^- \quad (7a)$$

$$NO_3^- + V_O^+ \leftrightarrow NO + 2O^- + V_O^{2+} \quad (7b)$$

When O^- pressure increases, the resistance of the material also increases in a n-type semiconductor, as experimentally observed, except with lithium doping.

5. Conclusions

Alkaline (lithium, potassium, rubidium) and alkaline-earth (magnesium, barium) doped hematite were investigated for NO_2 sensing applications. As a comparison, pure hematite material was also studied under the same conditions. Electrical characterizations were performed by AC impedance spectroscopy under various temperatures and gas atmospheres. SEM analysis and electrical conductivity under air and argon revealed that ferrites of potassium and rubidium were not stable.

Lithium, magnesium and barium doped hematite materials showed an extrinsic n-type semiconducting behavior for temperature below 500 °C.

The study under NO_2 environment revealed that lithium doped hematite exhibited a singular behavior we could explain on the basis of a transition from n-to p-type conductivity due to the formation of an inversion layer. On the contrary, magnesium and barium doped hematite showed the attempt resistance increase with NO_2 partial pressure. The remarkable linearity of these latter material responses is promising for the targeted application.

Acknowledgements

C. Baroni is grateful to Piedmont Region and to INSTM (Inter-University National Consortium on Material Science and Technology) for partial financial support of her Ph.D. grant.

References

1. Directive 2008/50/EC of the European Parliament and of the Council of 21 May 2008 on ambient air quality and cleaner air for Europe. Off J Eur Union (11.06.2008) L152/1–44. Available online: http://eur-lex.europa.eu/LexUriServ/LexUriServ.do?uri=OJ:L:2008:152:0001:0044:EN:PDF.
2. Nenov TG, Yordanov SP. *Ceramic sensor – technology and applications*. Lancaster: Technomic Publishing Company; 1996.
3. Pelino M, Colella C, Cantalini C, Faccio M, Ferri G, D'Amico A. Microstructure and electrical properties of an α-hematite ceramic humidity sensor. *Sens Actuators B: Chem* 1992;**7**:464–9.
4. Traversa E. Ceramic sensors for humidity detection: the state-of-the-art and future developments. *Sens Actuators B: Chem* 1995;**23**:135–56.
5. Gusmano G, Montesperelli G, Morten B, Prudenziati M, Pumo A, Traversa E. Thick films of $MgFe_2O_4$ for humidity sensors. *J Mater Process Technol* 1996;**56**:589–99.
6. Shah J, Kotnala RK, Singh B, Kishan H. Microstructure-dependent humidity sensitivity of porous $MgFe_2O_4$–CeO_2 ceramic. *Sens Actuators B: Chem* 2007;**128**:306–11.
7. Neri G, Bonavita A, Galvagno S, Pace C, Patanè S, Arena A. Humidity sensing properties of Li–iron oxide based thin films. *Sens Actuators B: Chem* 2001;**73**:89–94.
8. Tulliani JM, Bonville P. Influence of the dopants on the electrical resistance of hematite-based humidity sensors. *Ceram Int* 2005;**31**:507–14.
9. Neri G, Bonavita A, Galvagno S, Donato N, Caddemi A. Electrical characterization of Fe_2O_3 humidity sensors doped with Li^+, Zn^{2+} and Au^{3+} ions. *Sens Actuators B: Chem* 2005;**111–112**:71–7.
10. Neri G, Bonavita A, Milone C, Pistone A, Galvagno S. Gold promoted Li–Fe_2O_3 thin films for humidity sensors. *Sens Actuators B: Chem* 2003;**92**:326–30.
11. Kotnala RK, Shah J, Singh B, Kishan H, Singh S, Dhawan SK, et al. Humidity response of Li-substituted magnesium ferrite. *Sens Actuators B: Chem* 2008;**129**:909–14.
12. Esteban-Cubillo A, Tulliani JM, Pecharromán C, Moya JS. Iron-oxide nanoparticles supported on sepiolite as a novel humidity sensor. *J Eur Ceram Soc* 2007;**27**:1983–9.
13. Ito S, Washio M, Makino I, Koura N, Akashi K. Role of potassium ions in humidity sensitivity of K+-β-ferrite. *Solid State Ionics* 1996;**86–88**:1005–11.
14. Pelino M, Cantalini C, Sun HT, Faccio M. Silica effect on α-Fe_2O_3 humidity sensor. *Sens Actuators B: Chem* 1998;**46**:186–93.
15. Sun HT, Cantalini C, Faccio M, Pelino M. NO_2 gas sensitivity of sol–gel-derived α-Fe_2O_3 thin films. *Thin Solid Films* 1995;**269**:97–101.
16. Cantalini C, Sun HT, Faccio M, Ferri G, Pelino M. Niobium-doped α-Fe_2O_3 semiconductor ceramic sensors for the measurement of nitric oxide gases. *Sens Actuators B: Chem* 1995;**25**:673–7.
17. Zhuiykov S, Ono T, Yamazoe N, Miura N. High-temperature NOx sensors using zirconia solid electrolyte and zinc-family oxide sensing electrode. *Solid State Ionics* 2002;**152–153**:801–7.
18. Neri G, Bonavita A, Galvagno S, Siciliano P, Capone S. CO and NO_2 sensing properties of doped-Fe_2O_3 thin films prepared by LPD. *Sens Actuators B: Chem* 2002;**82**:40–7.
19. Jing Z. Synthesis, characterization and gas sensing properties of undoped and Zn-doped γ-Fe_2O_3-based gas sensors. *Mater Sci Eng A* 2006;**441**:176–80.
20. Ivanovskaya MI, Kotsikau DA, Taurino A, Siciliano P. Structural distinctions of Fe_2O_3–In_2O_3 composites obtained by various sol–gel procedures, and their gas sensing features. *Sens Actuators B: Chem* 2007;**124**:133–42.
21. Seiyama T, Yamazoe N, Arai H. Ceramic humidity sensors. *Sens Actuators* 1983;**4**:85–96.
22. Traversa E, Bearzotti A. Humidity sensitive electrical properties of dense ZnO with non-ohmic electrode. *J Ceram Soc Jpn* 1995;**103**(1):11–5.
23. Han JS, Davey DE, Mulcahy DE, Yu AB. Effect of pH value of the precipitation solution on the CO sensitivity of α-Fe_2O_3. *Sens Actuators B: Chem* 1999;**61**:83–91.
24. Ivanovskaya M, Gurlo A, Bogdanov P. Mechanism of O_3 and NO_2 detection and selectivity of the In_2O_3 sensors. *Sens Actuators B: Chem* 2001;**77**:264–7.
25. Santilli CV, Bonnet JP, Dordor P, Onillion M, Hagenmuller P. Influence of structural defects on the electrical properties of α-Fe_2O_3 ceramics. *Ceram Int* 1990;**16**:25–32.
26. Kim KH, Lee SH, Choi JS. Electrical conductivity of pure and doped α-ferric oxides. *J Phys Chem Solids* 1985;**46**:331–8.
27. Gardner RFG, Sweett F, Tanner DW. The electrical properties of alpha ferric oxide-II. Ferric oxide of high purity. *J Phys Chem Solids* 1963;**24**:1183–96.
28. Chang RH, Wagner JB. Direct-current conductivity and iron tracer diffusion in hematite at high temperatures. *J Am Ceram Soc* 1972;**55**:211–3.
29. Stone HEN. Electrical conductivity and sintering in iron oxides at high temperatures. *J Mater Sci* 1968;**3**:321–5.
30. Dudley GJ, Steel BCH, Howe AT. Studies of potassium ferrite $K_{1+x}Fe_{11}O_{17}$. I. Electronic conductivity and defect structure. *J Solid State Chem* 1976;**18**:141–7.
31. Ito S, Kurosawa H, Akashi K, Michiue Y, Watanabe M. Crystal structure and electric conductivity of K+-β-ferrite with ideal composition $KFe_{11}O_{17}$. *Solid State Ionics* 1996;**86–88**:745–50.
32. Michel A. Ferrites. In: Pascal P, (Eds.) Nouveau traité de chimie minérale. Tome XVII, Fer, Paris: Masson; 1967, p 689-751.
33. Gurlo A, Sahm M, Oprea A, Barsan N, Weimar U. A p- to n-transition on α-Fe_2O_3-based thick film sensors studied by conductance and work function change measurements. *Sens Actuators B: Chem* 2004;**102**:291–8.
34. Aono H, Hirazawa H, Naohara T, Maehara T. Surface study of fine $MgFe_2O_4$ ferrite powder prepared by chemical methods. *Appl Surf Sci* 2008;**254**:2319–24.
35. Berger O, Hoffmann T, Fischer WJ, Melev V. Tungsten-oxide thin films as a novel materials with high sensitivity to NO_2, O_3, and H_2S Part II: application as a gas sensors. *J Mater Sci – Mater Electron* 2004;**15**:483–93.
36. Chiorino A, Ghiotti G, Prinetto F, Carotta MC, Gnani D, Martinelli G. Preparation and characterization of SNO_2 and MoOx–SnO nanosized powders for thick film gas sensors. *Sens Actuators B: Chem* 1999;**58**:338–49.